Ther Adv Neurol Disord
2019, Vol. 12: 1–18
DOI: 10.1177/1756286419859725

Therapeutic effect on experimental acute cerebral infarction is enhanced after nanoceria labeling of human umbilical cord mesenchymal stem cells

Lian Zuo, Qishuai Feng, Yingying Han, Mengwei Chen, Mengruo Guo, Zhongmin Liu, Yu Cheng and Gang Li

Abstract

Background: Therapeutic applications of stem cells, especially mesenchymal stem cells, were once regarded as a promising therapy for mitigating acute cerebral infarction. Unfortunately, all the stem cell clinical trials have been futile. A new stroke therapeutic strategy of combining stem cells with nanotechnology has recently gained significant attention. The objective of this study was to evaluate the application of cerium oxide nanoparticle (nanoceria)-labeled human umbilical cord mesenchymal stem cells (HucMSCs) for stroke therapy.

Methods: In our study, cerium oxide nanoparticles were precovered with hyaluronic acid before labeling HucMSCs and the synergistic effects from both HucMSCs and cerium oxide nanoparticles were analyzed in *in vivo* and *in vitro* experiments

Results: The nanoceria-labeled HucMSCs combined advantages from both sides, including the capacity for inflammatory modulation of HucMSCs and the antioxidant effects of nanoceria. Compared with either HucMSCs or nanoceria individually, nanoceria-labeled HucMSCs exerted significantly enhanced capacities after gaining combined antioxidant and anti-inflammatory effects.

Conclusion: Our findings suggest a novel strategy with effective and well-tolerated applications of stem cells for acute cerebral infarction therapy after modification of cells with nanomaterials.

Keywords: acute cerebral infarction, anti-inflammatory, antioxidant, human umbilical cord mesenchymal stem cells, nanoceria

Received: 31 March 2019; revised manuscript accepted: 3 June 2019.

Correspondence to:
Gang Li
Department of Neurology,East Hospital, Tongji University School of Medicine, Shanghai, 200120, China
ligang@tongji.edu.cn

Yu Cheng
East Hospital; The Institute for Biomedical Engineering & Nano Science, Tongji University School of Medicine, Shanghai, 200120, China
yucheng@tongji.edu.cn

Zhongmin Liu
Department of Intensive Care Center, East Hospital, Tongji University School of Medicine, Shanghai, 200120, China
liu.zhongmin@tongji.edu.cn

Lian Zuo
Yingying Han
Mengruo Guo
Department of Neurology, East Hospital, Tongji University School of Medicine, Shanghai, China

Qishuai Feng
Department of Neurology, East Hospital, Tongji University School of Medicine, Shanghai, China;
East Hospital, The Institute for Biomedical Engineering and Nano Science, Tongji University School of Medicine, Shanghai, China

Mengwei Chen
East Hospital, The Institute for Biomedical Engineering and Nano Science, Tongji University School of Medicine, Shanghai, China

Introduction

Acute cerebral infarction (ACI) is a severe neurological disease with high disability worldwide. Currently, intravenous thrombolysis and endovascular intervention are clinically applicable treatments for ACI. However, both treatments have significant clinical limitations; they are only applicable either in the early stage of ischemic stroke or in a selective group of patients with stroke. Intravenous thrombolysis has a narrow therapeutic window, within 4.5 h after the onset of ACI.[1] Although endovascular intervention may be employed within 24 h after the onset of ischemic stroke in a strictly selected group of patients,[2,3] special devices and professional endovascular intervention specialist are required. Therefore, there is an urgent need of exploring other effective treatments for ACI.

Stem cell therapy after stroke has been regarded as a promising strategy to replace stroke-damaged tissue and to regain neurological function.[4]

Neural stem cells (NSCs) are present in various parts of the central nervous system including the subventricular zone (SVZ) and subgranular zone (SGZ) of the dentate gyrus.[5] However, the regeneration capacities of NSCs are inadequate for reparation or replacement of damaged brain tissues after stroke.[6] For that reason, stem cell research in the stroke field has been focused on exogenous stem cell therapy. Mesenchymal stem cell (MSC) preparations are available from various donor tissues, and have low immunogenicity and minimal ethical concerns.[7,8] Preclinical trials in animal models indicate that MSCs offer neuroprotection, angiogenesis and neurogenesis, probably *via* the modulation of the immune response.[9–12] Clinical studies revealed the safety and feasibility in the MSC treatment of ischemic stroke.[13–17] However, meta-analysis indicates that the efficacy of the MSC treatment of ischemic stroke remains uncertain.[18,19] Recent studies indicate that MSCs, which either overexpress growth factors or are preconditioned by drugs or combine with hypothermia, may enhance their beneficial effects.[20–25] Indeed, these pretreatments of MSCs did increase the immunomodulatory features of MSC. However, these modified or preconditioned MSCs may still be inadequate for offering clinical benefits after ischemic stroke.

Cerium oxide nanoparticles (nanoceria) can reversibly bind to oxygen molecules, thus making a shift between Ce^{3+} (reduced, electron donor) and Ce^{4+} (oxidized, electron acceptor) on the surface of the particles. For that reason, nanoceria may scavenge intracellular reactive oxygen species (ROS).[26] Nanoceria may exert multiple effects under several disease conditions, including antioxidative stress,[27] anti-inflammation,[28] neuroprotection[29,30] and radioprotection.[31] The objective of this study was to investigate whether nanoceria may further enhance MSC neuroprotective benefits in an animal stroke model.

Materials and methods

Synthesis of nanoceria

Nanoceria were synthesized by high temperature decomposition as reported previously.[32] Briefly, 0.434 g of $Ce(NO_3)_3 \cdot 6H_2O$, 0.802 g of oleylamine and 4.0 g of 1-octadecene were mixed and sufficiently dissolved at room temperature. During 30 min stirring at 80°C, the mixture solution was changed from dark brown to a clear brownish yellow solution. And then the resulting solution was heated for 2 h at 260°C. The remaining chemicals were removed using a washing solution of 1:1 of methanol and acetone by centrifugation. Highly purified nanoceria were obtained and dispersed in hexane or chloroform for further experiments.

Hyaluronic acid-coated nanoceria

Nanoceria (5 mg, 1 mg/ml) were added to hyaluronic acid (25 mg, 5 mg/ml) in 30 ml of the solution with a mixture of hexane and ethanol. The reaction mixture was sonicated using a probe sonicator for 1 h at 40% amplitude and with cycles of 5 sec on and 2 sec off. Hexane and ethanol were removed by evaporation at 40°C. Purification of as-prepared hyaluronic acid-coated nanoceria (HA-CeO_2) were carried out using ultracentrifugation at 30,000 r/min for 30 min to remove the remaining hyaluronic acid. Finally, highly purified HA-CeO_2 pellets were dispersed in deionized water for further experiments.

Physicochemical characterization of HA-CeO_2

The physicochemical properties of HA-CeO_2 were determined by different physicochemical techniques. The morphology, size, shape, and energy-dispersive X-ray spectroscopy (EDX) were characterized by transmission electron microscopy (TEM); the hydrodynamic diameters and surface charge were determined by dynamic light scattering and zeta potential, respectively; Ce^{3+}/Ce^{4+} patterns were determined by X-ray photoelectron spectroscopy (XPS); the concentrations of HA-CeO_2 were calculated by inductively coupled plasma mass spectrometry (ICP-MS).

Cell culture

Human umbilical cord MSCs (HucMSCs) used in this study were kindly provided by Prof. Yufang Shi and his team (Institute of Health Sciences, Shanghai Institutes for Biological Sciences, Chinese Academy of Sciences, China). HucMSCs were grown in low glucose Dulbecco's modified Eagle's medium (LG-DMEM) containing 10% fetal bovine serum, 1% penicillin and 1% streptomycin, and incubated in a humidified atmosphere (5% CO_2) at 37°C.

Cell viability test in MTT assay

Cell viability was determined at 24 h after HA-CeO_2 treatment using the MTT method, according to the manufacture protocols (R&D, Minnesota, USA). Briefly, HucMSCs were seeded into 96-well plates at a density of 5×10^3 cells per well. After incubating overnight, the cells were treated with HA-CeO_2 at a series of Ce concentrations (0.1, 1, 10, 25, 75, 150 and 300 μM). After 24 h incubation, MTT reagent (0.5 mg/ml, final concentration) was added into each well and incubated with HucMSCs for 4 h at 37°C and 5% CO_2. The absorbance of the culture media was measured at 570 nm. The viabilities of the treated groups were evaluated based on the control group without HA-CeO_2 treatment (ELx808, BioTek).

C-X-C chemokine receptor type 4 expression of HucMSCs determined in western blot

To reveal C-X-C chemokine receptor type 4 (CXCR4) expression of HucMSCs with HA-CeO_2 treatment, HucMSCs were incubated without or with HA-CeO_2 (25, 50, 150 μM) for 24 h. Then, cells were washed twice with phosphate-buffered saline (PBS). After the collection of cells, whole cell lysates were obtained using a cell lysis buffer (Beyotime, China). CXCR4 expression of HucMSCs was determined by western blot with antibody (R&D).

HucMSCs migration ability determined by wound healing assay

The wound healing assay was performed for the migration ability of HucMSCs after HA-CeO_2 treatment. A linear wound was made by ibidi Transwells. Cells were planted into both sides of the linear wound at a density of 3×10^5 per well. Cells were incubated with the different concentrations of HA-CeO_2 (25, 50, 150 μM). After 24 h, the media were washed twice with PBS and then fresh medium was added for 24 h. Finally, all of the analyzed cells were visualized by Live Cell Station (EVOS FL Auto, Life Technologies).

Characterization of HucMSCs by flow cytometry

The stemness of HucMSCs with HA-CeO_2 was characterized by flow cytometry (Attune®NxT flow cytometer, Thermo Fisher, USA). Briefly, cells were plated into a 12-well plate at a density of 1×10^5 per well overnight. Then cells were treated with 50 μM HA-CeO_2 for 24 h. Cells were stained with the following antibodies (positive markers: CD29-APC, CD44-BV421, CD90-FITC, CD105-PerCP-Cy5.5; negative markers: CD34-PE, CD45-PE), and then analyzed by flow cytometry. The data were analyzed with FlowJo software.

Cellular uptake and internalization of nanoceria

The uptake efficiency of HucMSCs with HA-CeO_2 was examined by flow cytometry. HucMSCs were seeded into 12-well plates at a density of 5×10^4 cells per well and kept overnight. Next, the growth medium was replaced with the treatment media of Cy5.5-HA-CeO_2 (Ce concentration at 50 μM) at time points of 4, 24, and 36 h. After incubation, cells were detached with 200 μl trypsin-ethylenediaminetetraacetic acid (EDTA). Cells were pelleted and washed with PBS at least three times. Finally, cells were resuspended in 0.5 ml of PBS for flow cytometry assay.

Cellular internalization of HA-CeO_2 was analyzed by using confocal fluorescence microscopy. HucMSCs were seeded onto a confocal microscopy dish (NEST) at a density of 5×10^4 cells per well. After culturing for 4, 24, and 36 h, the cells were treated with Cy5.5-HA-CeO_2 (50 μM Ce concentration) for 4 h. The cells were washed twice using PBS (pH 7.4), stained with Lyso Tracker Green (1:10,000 dilution; Life Technologies, USA) and stored in an incubator at 37°C for 30 min. The cultures were then washed twice with PBS on ice and immediately observed using laser scanning confocal microscopy (Leica TCS SP5, Germany). HucMSCs were then stained with 4′6- diamidino-2-phenylindole (DAPI) for 10 min at room temperature. Finally, the cultures were washed with 1 ml PBS. The fluorescence emission spectra of Cy5.5 (Ex/Em = 673/707 nm) and DAPI (Ex/Em = 350/461 nm) were immediately captured using a confocal microscope.

Antioxidant ability of HA-CeO_2 was analyzed via *scavenged intracellular ROS*

The intracellular ROS was assayed by the cell-permeable and oxidation-sensitive 2,7-dichlorodihydrofluorescein diacetate (DCFH-DA). DCFH-DA is the most widely used cell-permeable probe for detecting intracellular oxidative stress. DCFH-DA is hydrolyzed intracellularly to

become the fluorescent product dichlorofluorescein (DCF), which is retained inside the cells.[29] The intracellular ROS production in astrocytes was induced by different doses of H_2O_2 (62.5–1000 μM) to confirm the optimal H_2O_2 dose.

The ROS-scavenging effect of HA-CeO_2 was evaluated in the cell culture model of HucMSCs and astrocytes treated with optimal H_2O_2. A total of 5×10^3 HucMSCs and the same number of astrocytes were seeded separately per well on a 96-well plate for 24 h. Cell media were replaced with fresh media containing different concentrations of HA-CeO_2 (75, 150, 300 μM). After 24 h incubation, the cells were washed by PBS and then 100 μl of fresh media (free serum) with 250 or 500 mM H_2O_2 was added into each well and incubated for 30 min. After that, 100 μl of fresh media (free serum) containing 50 μM DCFH-DA solution was added to each well and incubated for 60 minutes at 37°C. The fluorescence imaging was recorded using Live Cell Station.

To determine the anti-apoptotic activity of HA-CeO_2, a Caspase-3/7 Green Flow Cytometry Assay Kit was used to detect the caspase-3/7 activity by flow cytometry (Attune®NxT flow cytometer, Thermo Fisher).

In vivo experiments of a rat model

Animals

Specific pathogen-free Sprague–Dawley rats were housed in a 12 h light/dark cycle with access to food and water *ad libitum*. All animal procedures were conducted in accordance with guidance for the Care and Use of Laboratory Animals of Tongji University and were approved by the committee of experimental animals of Tongji University. Rats with 240–280 g body weight (7–8 weeks old) were used for this study.

Middle cerebral artery occlusion model

Rats were anesthetized intraperitoneally with pentobarbital sodium (40 mg/kg). The rats were subjected to middle cerebral artery occlusion (MCAO) according to the method described previously.[33,34] Regional cerebral blood flow (CBF) was monitored by laser Doppler flowmetry of the Periflux system 5000 (Preimed, Sweden) with the use of a probe placed over the skull to confirm at least 70% reduction of the CBF. After 120 min of MCAO, the monofilament was removed to restore middle cerebral artery blood flow.

A total of 156 rats had established MCAO during this research. Among them, 32 rats were used for evaluation on the establishment of an optimal dose (see supplementary material). All other 124 rats were used for analyzing the effects of HA-CeO_2-labeled HucMSCs as follows: 20 rats (5 rats in each group) were harvested 2 days after MCAO, 40 rats (10 rats in each group) were harvested 3 days after MCAO. The remaining 64 rats were used to record the weight, survival status and neurological examination till 7 days after MCAO.

Neurologic examination and group allocation

Neurologic impairment was evaluated 24 h and 7 days after cerebral reperfusion using a Bederson 4-point score and Garcia 18-point score.[35] In order to find the optimal dose of HucMSCs for transplantation, HucMSC doses of 1×10^6, 2×10^6 and 4×10^6 were first evaluated after transplantation into MCAO rats. Then, neurologic scores and morphological changes of infarct areas were compared, which confirmed the HucMSC dose of 2×10^6 was optimal for transplantation into MCAO rats (see supplementary material). Rats were randomly divided into four groups after the first neurologic examination: (1) MCAO + 0.5 ml normal saline (NS) group as control; (2) MCAO + HucMSC group (each rat received 2×10^6 HucMSCs); (3) MCAO + HA-CeO_2 group (each rat received 0.5 mg/kg HA-CeO_2 according the previous report[30]) and MCAO + HA-CeO_2-labeled HucMSC group (2×10^6 HucMSC-labeled 0.5 mg/kg HA-CeO_2). HucMSCs and HA-CeO_2 were suspended in 0.5 ml NS and transplanted *via* the caudal vein into rats. Each rat of the control group received 0.5 ml NS. The body weights and death of animals were recorded daily.

Measurement of infarct area

At Day 7 after MCAO, rats were anesthetized with an overdose of pentobarbital sodium and the brains were rapidly removed and frozen at −20°C for 15 min. Then the brains were sliced into seven serial 2-mm coronal sections and incubated in 2% 2,3,5-triphenyltetrazolium chloride (TTC; Sigma, USA) at 37°C for 10 min. The extent of the infarction area and normal brain area were outlined manually and calculated using ImageJ software (National Institutes of Health, version

Table 1. The sequences of primers for real-time quantitative polymerase chain reaction.

Symbol	Forward primer	Reverse primer	Fragment length
iNOS	GCAGGTTGAGGATTACT	CTTTTTTGCTCCATAGG	91bp
BDNF	GGAAAGGGTGAAACAAAG	GTGGGACTCCAGAAGACA	118bp
GDNF	AGAGGGAAAGGTCGCAG	AGCCCAAACCCAAGTCA	91bp
Prdx6	GTTGACTGGAAGAAGGG	GGAAAAGTTGTTTGGCT	73bp
NF-κB	TAAACCAAAGCCCTGAAAG	CAGAGCCAAGAAAGGAAGC	145bp
NT-3	GATCCAGGCGGATATCTTGA	AATCATCGGCTGGAATTCTG	145bp
NGF	CAACAGGACTCACAGGAGCA	GTCCGTGGCTGTGGTCTTAT	115bp
VEGF	GGAGGATGTCCTCACTTGGA	CAAACAGACTTCGGCCTCTC	97bp
Nrf2	GGAGCAATTCAACGAAGCTC	ACAGTTCTGAGCGGCAACTT	82bp
GAPDH	TCCTGCACCACCAACTGCTTAG	AGTGGCAGTGATGGCATGGACT	102bp

BDNF, brain-derived neurotrophic factor; GAPDH, glyceraldehyde phosphate dehydrogenase; GDNF, glial-derived neurotrophic factor; iNOS, inducible nitric oxide synthase; NF-κB, nuclear factor κB; NGF, nerve growth factor; Nrf2, nuclear factor-erythroid-2-related factor 2; NT-3, neurotrophin 3; Prdx6, peroxiredoxin 6; VEGF, vascular endothelial growth factor.

1.44). The infarction volumes were expressed as the total infarct area multiplied by the thickness of brain sections. To evaluate the effect of correcting acute brain edema, the lesion volume was determined as: the corrected infarct area = [infarct − (ipsilateral hemisphere − contralateral hemisphere)]/contralateral hemisphere × 100, as described previously.[36–38]

Real-time quantitative polymerase chain reaction

Total RNA was isolated from the infarct and surrounding tissues of each individual rat ($n=5$) at Days 3 and 7 after MCAO by using TRIzol Reagent (Invitrogen, USA). Real-time quantitative polymerase chain reaction (PCR) was performed using the Applied Biosystems real-time Prism 7900 HT Sequence Detection System (ABI, USA). The sequences of primers are listed in Table 1.

ROS measurement

Rat brain tissues from each group at Days 2, 3 and 7 ($n=5$) after MCAO were harvested and all procedures were done as the instructions in the rat ROS enzyme-linked immunosorbent (ELISA) kit (R&D). Details are available from the supplementary data.

Cytokine measurements

Rat brain tissues homogenates from each group at Days 2, 3 and 7 ($n=5$) after MCAO were analyzed and assayed for cytokines using multiplexed bead-based immunoassay kit for rats including interleukin (IL)-1β, IL-4, IL-6, IL-10, interferon (IFN)-γ, tumor necrosis factor (TNF)-α, monocyte chemotactic protein (MCP)-1, macrophage inflammatory protein (MIP)-1α, vascular endothelial growth factor (VEGF) and regulated upon activation normal T-cell expressed and secreted (RANTES) combined with a reagent kit (Bio-Rad, #171-304070). All procedures were done as per manual instructions and details are available from the supplementary data.

Apoptosis

Apoptotic cells of rat brain tissues from each group at Days 3 ($n=5$) after MCAO were analyzed by a TUNEL kit (Roche, Switzerland). Brain tissues embedded in paraffin were cut in 4-μm thick slices. Labeled apoptotic cells were identified by treating the sections with the peroxidased chromogenic substrate 3,3′-diaminobenzidine (DAB) as recommended in the kit. Overall, five random selective observed fields of each slice were photographed under light microscopy with magnification ×200 and the apoptotic cells were

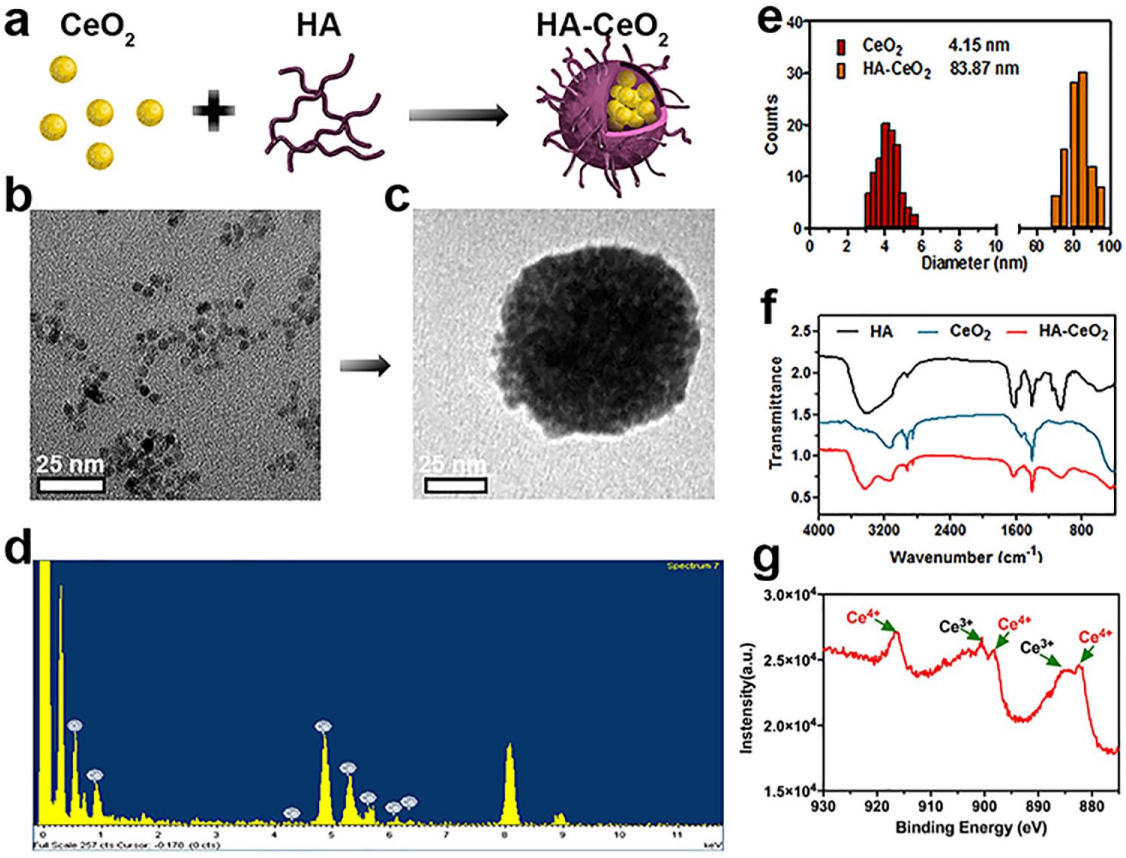

Figure 1. Synthesis and characterization of HA-CeO_2 (nanoceria). (a) Schematic synthesis of HA-CeO_2 nanoparticles. (b, c) TEM image of$CeO_2$and HA-CeO_2 nanoparticles (scale bar = 25 nm). (d) EDX analysis of HA-CeO_2. (e) Hydrodynamic diameters of CeO_2 and HA-CeO_2 nanoparticles. (f) FTIR analysis of HA, CeO_2 andHA-CeO_2. (g) XPS analysis of HA-CeO_2 identifies the valence state of cerium ions and confirms corresponding binding energy (BE) peaks for Ce^{3+} (880.20, 885.00, 899.50, and 903.50 ev) and Ce^{4+} (882.10, 888.10, 898.00, 900.90, 906.40, and 916.35 ev).
HA, hyaluronic acid; CeO_2, nanoceria; TEM, transmission electron microscopy; EDX, energy-dispersive X-ray spectroscopy; FTIR, Fourier Transform Infrared; XPS, X-ray photoelectron spectroscopy.

counted with Image-Pro Plus software (Media Cybernetics, version 6.0). The percentage of apoptotic cells to normal cells were summed then averaged in each group.

Statistical analysis

All statistical analyses were performed using GraphPad Prism software (GraphPad software, version 5.0). Presented data are reported as means ± standard error of the mean. A p value <0.05 was considered significant.

Results

Synthesis and characterization of the HA-CeO_2 (nanoceria) capable of HucMSC labeling

TEM images revealed discrete and uniform of 4.15 nm-sized nanoceria. After transfer to water, these nanoceria were assembled to form a nanocluster-like structure by the 90–172 kDa hyaluronic acid (HA) as HA-CeO_2 [Figure 1(a–c)]. Hydrodynamic diameters increased from 4.15 nm for ceria to the levels up to 100 nm for nanoceria at various assembly stages, and their zeta potential changes from 10 to 25 mV [Figure 1(d and e)]. Results from Fourier transform infrared (FTIR) analyses confirmed the successful conjugation of HA onto the nanoceria [Figure 1(f)]. Selected XPS segments relative to the valence states of cerium ions with corresponding binding energy peaks for Ce^{3+} (880.20, 885.00, 899.50, and 903.50 ev) and Ce^{4+} (882.10, 888.10, 898.00, 900.90, 906.40, and 916.35 ev) were also confirmed in both Ce^{3+} and Ce^{4+} nanostructures. Furthermore, the XPS analysis calculated the Ce^{3+} percentage of 39.8% [Figure 1(g)]. It was

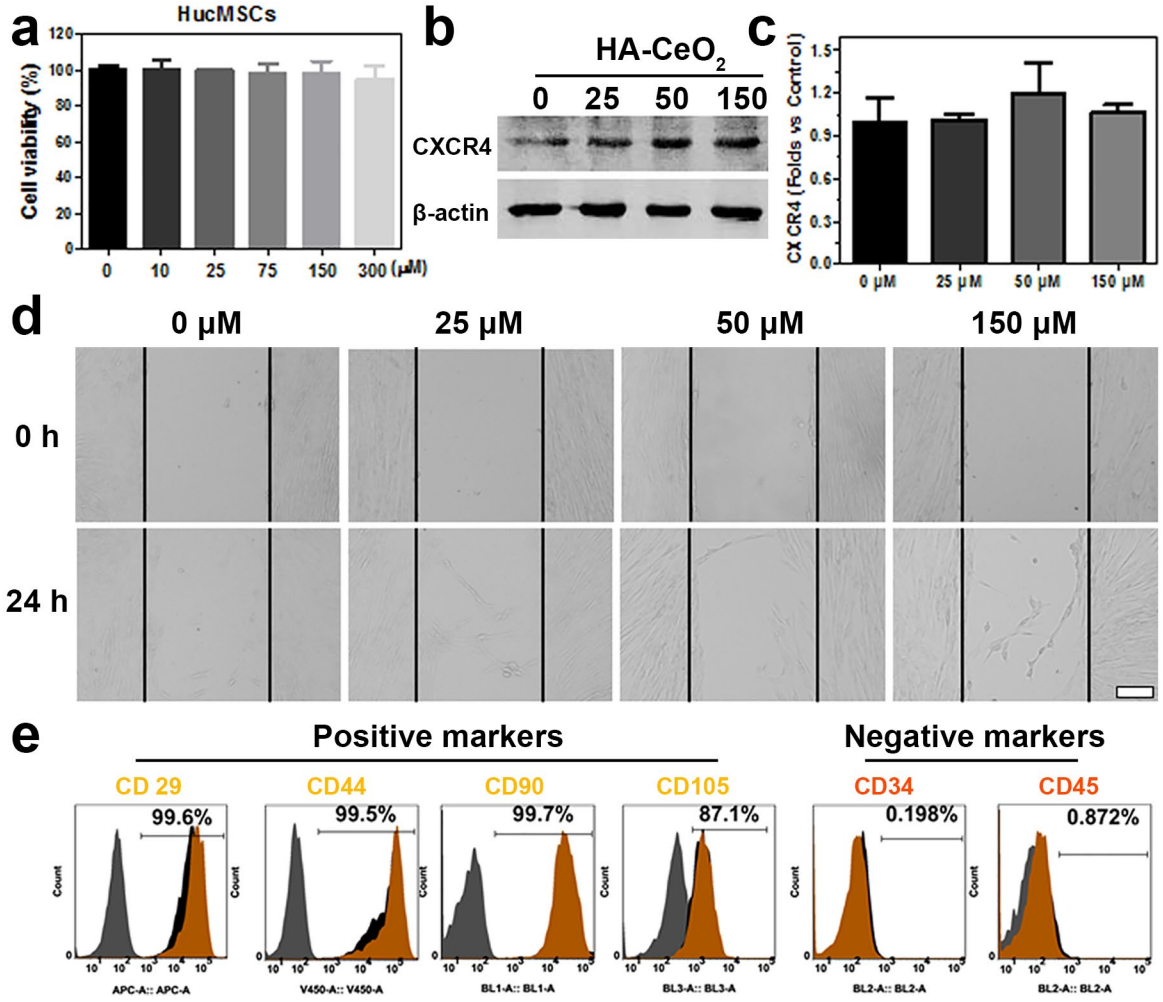

Figure 2. Effects of HA-CeO2 (nanoceria) on HucMSCs properties. (a) Cell cytotoxicity was determined by MTT assay after 24 h for the treatment with different concentrations of HA-CeO_2. (b, c) CXCR4 expression of HucMSCs with HA-CeO_2 labeling was performed by western blot analysis, β-actin as control. (d) Wound healing in HucMSCs without (control) or with different HA-CeO_2 concentrations shown by confocal laser scanning microscopy. Scale bar: 200 μM. (e) Flow cytometry analyses of the surface markers of HucMSCs without (control) or with 50 Mm of HA-CeO_2 after 24 h treatment.
MTT, methyl thiazolyl tetrazolium; CXCR4, C-X-C chemokine receptor type 4; HucMSCs, Human umbilical cord mesenchymal stem cells.

known that the nanoceria with a higher Ce^{3+} to Ce^{4+} ratio were more effective against the diseases associated with oxidative stress or inflammation, owing to their higher oxygen vacancy and superoxide dismutase (SOD) mimetic activity.

Biocompatibilities were proved after HucMSCs labeling with HA-CeO_2

Results of the MTT assay proved that there was no significant difference for the viabilities of HucMSCs at 24 h after labeling with HA-CeO_2 at a series of concentrations from 0 μM to 300 μM [Figure 2(a)]. Under the same situations, the expression levels of CXCR4 protein in HucMSCs with HA-CeO_2 at several concentrations (25, 50, and 150 μM) indicated that the CXCR4 expression levels had no significant difference, suggesting that HA-CeO_2 labeling did not influence CXCR4 protein expression in HucMSCs [Figure 2(b, c)]. Furthermore, our results also showed that HA-CeO_2 had no effect on HucMSCs migration [Figure 2(d)]. Finally, results of phenotypic analyses on the surface markers indicated that positive staining for CD29, CD44, CD90 and CD105 and negative staining for CD45 and CD34 were achieved on both nonlabeled HucMSC controls and labeled HucMSC at 24 h

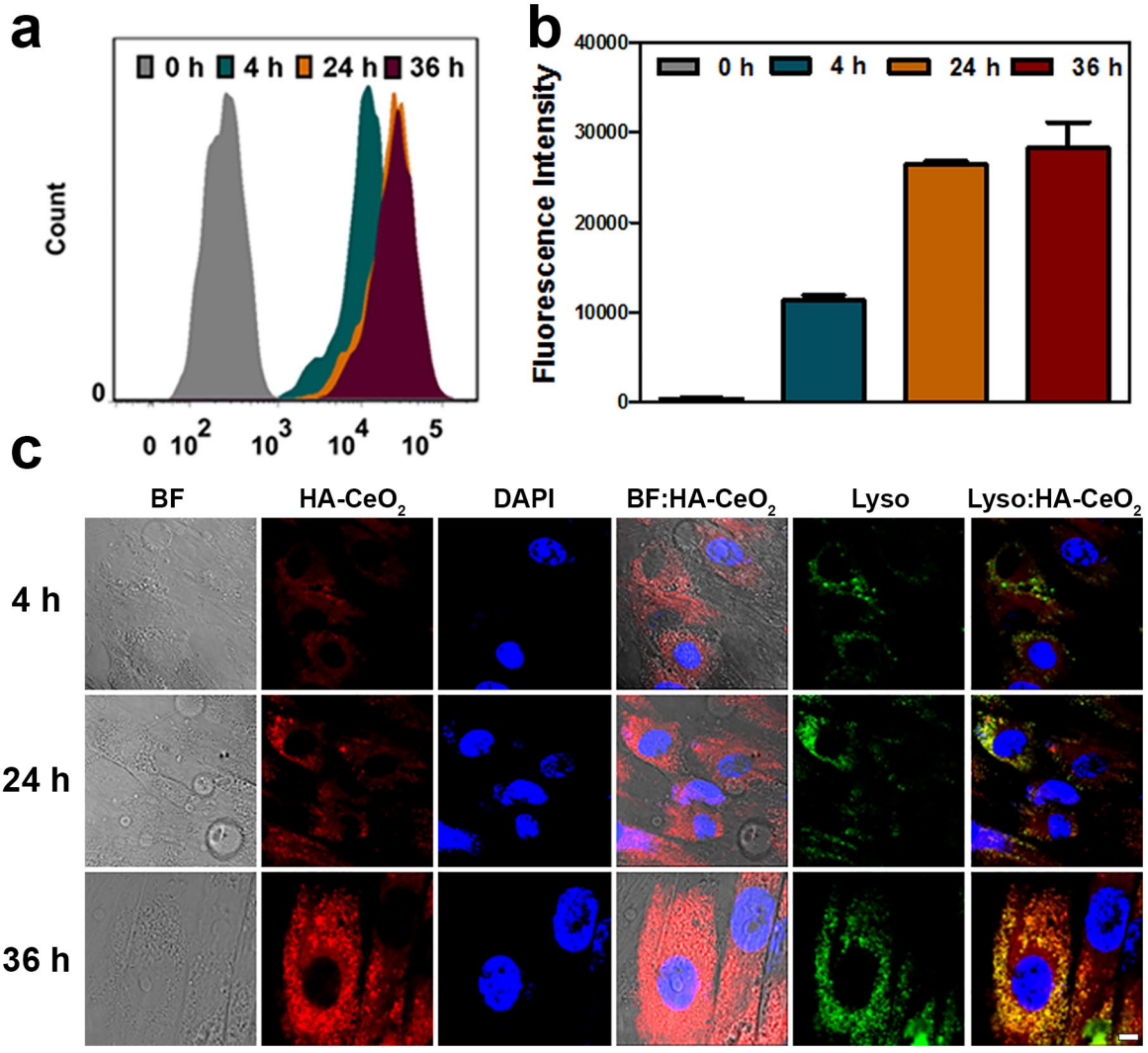

Figure 3. Intracellular distribution of HA-CeO_2 (nanoceria) in HucMSCs. (a) Flow cytometry analysis of HucMSCs before (0 h) and following incubation with Cy5.5-HA-CeO_2 for 4 h, 24 h and 36 h. (b) Quantitative analysis of fluorescence intensity of the cellular Cy5.5-HA-CeO_2. (c) Confocal analysis for cellular accumulation and distribution of Cy5.5-HA-CeO_2 in HucMSCs at Ce concentration of 50 μM for 4 h, 24 h and 36 h. Scale bar: 10 μM.
HA, hyaluronic acid; CeO_2, nanoceria; HucMSCs, Human umbilical cord mesenchymal stem cells; Cy, Cyanine.

after HA-CeO_2 incubation [Figure 2(e)]. These results suggested that there was no obvious effect of HA-CeO_2 on surface marker expression. Therefore, the biocompatibility of nanoceria was systematically proven by various parameters as multiple evidence, which supported their potential clinical applications in future.

Cellular uptake and internalization of the HA-CeO_2 after labeled on HucMSCs

HA-CeO_2 was conjugated with Cy5.5 to become Cy5.5-HA-CeO_2. In order to determine the cellular uptake of HA-CeO_2 into HucMSCs, the analyzed cells were incubated with Cy5.5-HA-CeO_2 for 36 h. Results of flow cytometry analysis showed that more than 95% of HucMSCs was labeled by Cy5.5-HA-CeO_2 after 4 h [Figure 3(a)], and that labeling intensity reached to the higher levels at both 24 and 36 h [Figure 3(b)]. In order to determine cellular internalization of HA-CeO_2, the medium of Cy5.5-HA-CeO_2 was prepared for Ce concentration at 50 μM. After HucMSCs were incubated for 4 h, 24 h and 36 h, cell images were analyzed with confocal microscopy. Results indicated that the bright fluorescence signals of

the particles (red) were mainly distributed in the membrane and cytoplasm of HucMSCs [Figure 3(c)]. Together, our results proved that treatment for 24 h was an optimal duration for HA-CeO_2 labeling on HucMSCs to reach to the highest labeling intensity with the shortest time.

Capacities of antioxidant and anti-apoptosis for HA-CeO_2 were via scavenging the intracellular ROS

The level of generation of ROS was evaluated in both HucMSCs and astrocytes under *in vitro* culture conditions. Results indicated that the fluorescence density level for monitoring intracellular levels of ROS generation significantly increased in a trend of gradual increase along with increases in H_2O_2 dose from 62.5 μM to 1000 μM, when compared with the control [Figure 4(a, b)]. The results also suggested that treatments with H_2O_2 at doses from 250 to 500 μM were sufficient to generate the significant level of ROS. Therefore, H_2O_2 at doses of both 250 μM and 500 μM were chosen as the standard doses of H_2O_2 treatment for further studies.

To assess the antioxidant activity of HA-CeO_2, the intracellular ROS-scavenging activity was measured to determine whether HA-CeO_2 could decrease ROS production induced by H_2O_2. Results revealed that there were significant decreases in levels of ROS at different concentrations HA-CeO_2, when compared with controls that were either only incubated with H_2O_2 or without HA-CeO_2 treatments [Figure 4(c)]. The results suggested that HA-CeO_2 supplied a remarkable suppressive effect on intracellular ROS generation. During the processes, HA-CeO_2 preferentially scavenged the intracellular ROS in both HucMSCs and astrocytes.

Remarkably, the anti-apoptosis capacity of HA-CeO_2 was further evaluated by cleaved caspase-3/7, an important mediator of cell apoptosis used as a parameter inflow cytometry. Results showed that cleaved caspase-3/7 expressions in both HucMSCs and astrocytes were inhibited after treatments of HA-CeO_2 at concentrations of 75, 150 and 300 μM, which were significantly lower than those of the control activated by H_2O_2 [Figure 4(d)]. Taking together, the decreases in ROS production and caspase-3/7 expression effectively clarified both antioxidative and anti-apoptosis abilities for HA-CeO_2.

HA-CeO_2-labeled HucMSCs improved survival, healthiness and neurologic evaluation score in rat model of MCAO

The effect of HA-CeO_2-labeled HucMSCs on cerebral infarction was evaluated in a rat model of MCAO in order to prove the beneficial effects on HA-CeO_2-labeled HucMSCs for the therapy of ACI. The parameters of both the weight and death of rats were recorded every day after the induction of MCAO. A total of three experimental groups, along with one control group, were established with a total of 64 rats. All four groups were observed from Day 1 to Day 7 after MCAO. At Day 7 after MCAO induction, there was no significant difference in the death rate among all four groups. Until Day 7, the death rate of each group was: HA-CeO_2-labeled HucMSCs group (1/16), HucMSC group (2/16) and HA-CeO_2 group (2/16) and when compared with the control group [3/16; Figure 5(c)]. In addition, animal weight was used as a parameter to evaluate the health status. Results showed that the animal weights in all four groups declined at an early stage from Day 1 to Day 5 after MCAO, and then increased from Day 5 to Day 6 after MCAO. The starting time point of the weight increase was earlier in the HA-CeO_2-labeled HucMSC group than all other three groups. The parameter of rat weight was significantly heavier in the HA-CeO_2-labeled HucMSC group than control group from Day 1 to Day 6 after MCAO ($p < 0.05$). Rat weight was also significantly heavier in the HA-CeO_2 group than the control group at both Day 1 and Day 2 after MCAO ($p < 0.05$).There was no significant difference in rat weight between the HucMSC group and the control group between Day 1 to Day 7 [Figure 5(e)].

Next, the Bederson neurologic score and Garcia scores were recorded for the evaluation of therapeutic effects. Results indicated that there was no significant difference between the Bederson neurologic score among the three treatment groups and the control group at Day 1 and Day 7 after MCAO. There was also no significant difference in Garcia scores among all four groups at Day 1. However, at Day 7 after MCAO, the Garcia neurologic score was significantly higher in the HA-CeO_2-labeled HucMSC group than the control group ($p < 0.05$), which was 12.3 ± 1.0 in the HA-CeO_2-labeled HucMSC group, 11.6 ± 1.2 in the HucMSC group and 12 ± 1.8 in the HA-CeO_2 group, when compared with 11.3 ± 1.0 in the control group [Figure 5(d)].

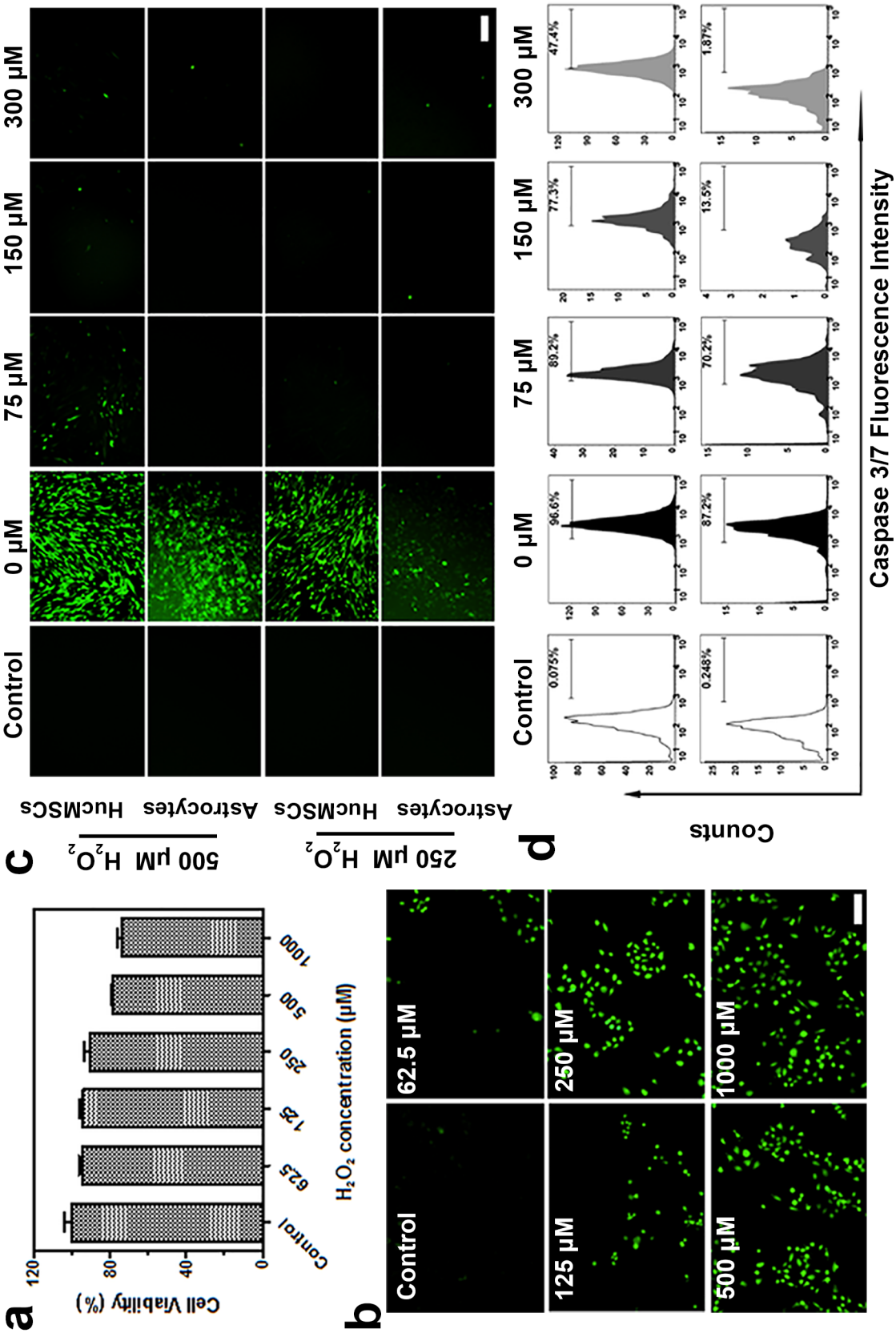

Figure 4. Antioxidant and anti-apoptosis ability of HA-CeO_2 (nanoceria) in HucMSCs and astrocytes. (a) Cell viability of HA-CeO_2 with a series of H_2O_2 concentrations after incubation for 1 h. (b) ROS were determined by staining with DCFH-DA in astrocytes with different H_2O_2 concentrations and observed by Live Cell Station. Scale bar: 100 μM. (c) Representative images of cellular ROS were perform by Live Cell Station in HucMSCs and astrocytes after HA-CeO_2 (75, 150 and 300 μM) and H_2O_2 (250 or 500 mM) using DCFH-DA. Scale bar: 100 μM. (d) Caspase 3/7 activation was assessed by flow cytometry using Cell Event Caspase-3/7 Green Detection Reagent.
HA, hyaluronic acid; CeO_2, nanoceria; HucMSCs, Human umbilical cord mesenchymal stem cells; ROS, Reactive Oxygen Species; DCFH-DA, 2,7-dichlorodihydrofluorescein diacetate

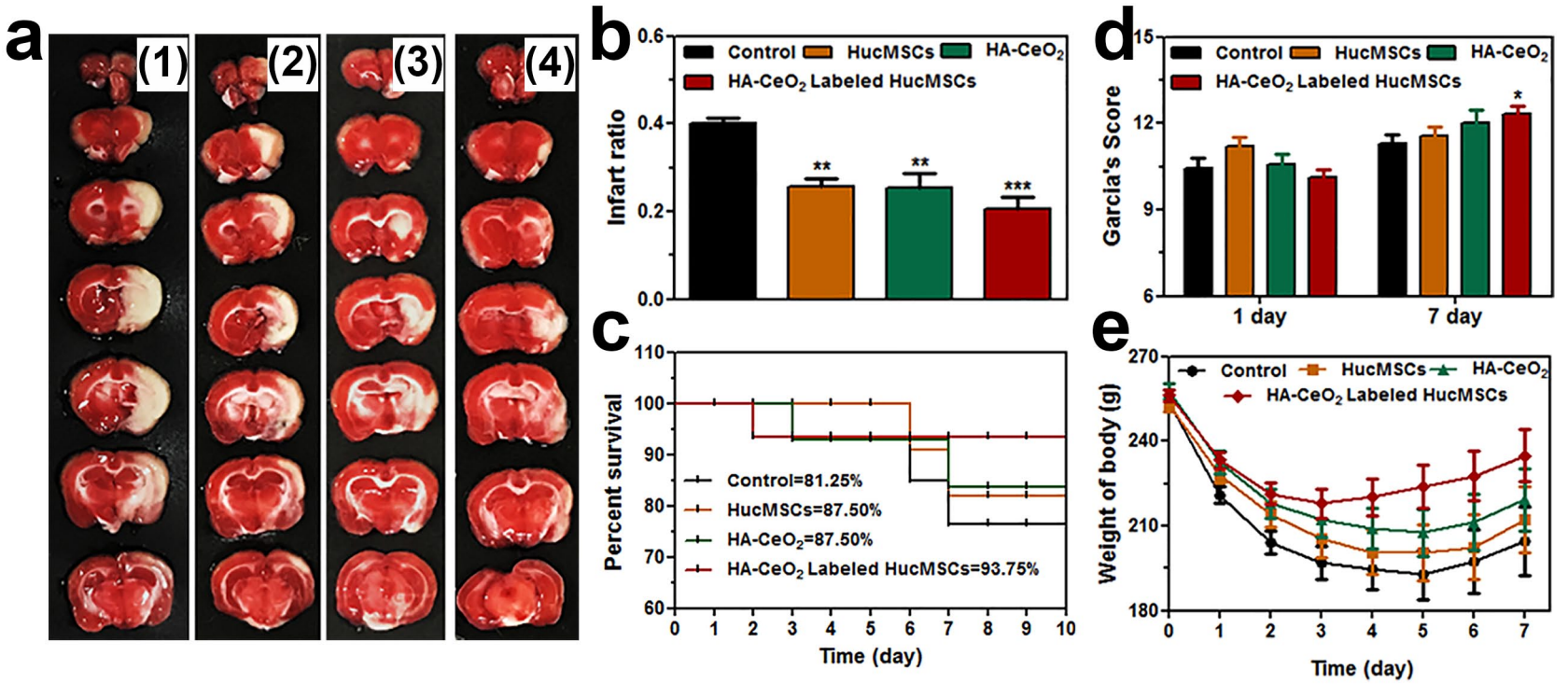

Figure 5. Enhanced therapy of HA-CeO_2 (nanoceria) labeled HucMSCs for ACI. (a) Representative image results of coronal brain sections using TTC staining. Representative coronal sections indicate the following groups: (1) MCAO + normal saline (control), (2) MCAO + HucMSCs, (3) MCAO+HA-CeO_2, and (4) MCAO + HA-CeO_2-labeled HucMSCs. (b)The bar chart shows the percentage of infarct volume of different groups. Error bars show the standard error, $^{**}p < 0.01$ *versus* the control group, $^{***}p < 0.001$ *versus* the control group. (c) Survival curve of MCAO rats of each group. (d) Garcia scales used to score animal behavior. The Garcia neurologic score at Day 7 after MCAO was significantly higher in the HA-CeO_2-labeled HucMSC group than the control group ($p < 0.05$). (e) The body weight variations of MCAO rats from different treatment groups. The weights of rats were significantly heavier in the HA-CeO_2-labeled HucMSC group than the control group during Day 1 to Day 6 after MCAO ($p < 0.05$). The weights of rats were significantly heavier in the HA-CeO_2 group than the control group at Day 1 and Day 2 after MCAO ($p < 0.05$).

HA, hyaluronic acid; CeO_2, nanoceria; HucMSCs, Human umbilical cord mesenchymal stem cells; ACI, Acute cerebral infarction; MCAO, middle cerebral artery occlusion; TTC, 2,3,5-triphenyltetrazolium chloride.

In summary, our results proved that HA-CeO_2-labeled HucMSCs significantly promoted the weight and neurological recovery and exhibited positive effects for rats after MCAO.

HA-CeO_2-labeled HucMSCs decreased infarct volume after MCAO

After TTC staining, the infarct area in the brain was white in color, while the normal tissue area was red in color [Figure 5(a)]. Remarkably, for infarction volume percentages, significant differences existed between each of three experimental groups and control group. The detailed results were summarized between the HA-CeO_2-labeled HucMSC group and control ($20.5 \pm 7\%$ *versus* $40.1 \pm 3\%$, $p < 0.01$, $n = 8$), between the HucMSC group and control ($25.6 \pm 5\%$ *versus* $40.1 \pm 3\%$, $p < 0.05$, $n = 8$) and between the HA-CeO_2 group and the control ($25.5 \pm 9\%$ *versus* $40.1 \pm 3\%$, $p < 0.05$, $n = 8$), respectively. The level of the infarction volume percentage was little smaller in the HA-CeO_2-labeled HucMSC group than the HA-CeO_2 group or HucMSC group [Figure 5(a, b)]. However, the overall differences among the three experimental groups were not significant. Together, these results of the TTC assay proved that HA-CeO_2-labeled HucMSCs helped to decrease the cerebral infarction volume effectively.

Enhanced antioxidative capacity of HA-CeO_2-labeled HucMSCs

To evaluate the effect of antioxidative stress of HA-CeO_2-labeled HucMSCs in transplanted MCAO rats, an ELISA was used to detect the levels of ROS expression in rat brain samples harvested at Days 2, 3 and 7 after MCAO. ROS expressions in the HA-CeO_2-labeled HucMSC group were significantly reduced at Day 7 compared with the control group [12.11 ± 0.83 IU/mg *versus* 27.64 ± 4.29 IU/mg, $p < 0.05$; Figure 6(i)]. Next, a real-time PCR assay was used to evaluate the expression levels of several genes relative to oxidative stress in the harvested rat brain tissues after MCAO, including inducible nitric oxide synthase (iNOS), nuclear factor-erythroid-2-related factor 2 (Nrf2) and peroxiredoxin 6 (Prdx6). Results indicated that the expressions of both iNOS and Prdx6 had no difference at Day 3 among all of four groups. However, iNOS gene expression declined differently at Day 7 in three experimental groups, which were 0.69 ± 0.15 in the HA-CeO_2-labeled HucMSC group, 0.68 ± 0.13 in the HucMSC group and 0.70 ± 0.15 in the HA-CeO_2 group. When compared with 1.01 ± 0.20 in the control group. Remarkably, the results of p values (HA-CeO_2-labeled HucMSCs *versus* control, $p = 0.035$; HucMSCs *versus* control, $p = 0.018$; HA-CeO_2 *versus* control, $p = 0.037$) indicated the specificities of significant differences [Figure 6(a)]. In addition, the expression level of the Nrf2 gene was significantly higher in the HA-CeO_2-labeled HucMSC group than both the HucMSC group (1.44 ± 0.28 *versus* 0.95 ± 0.08, $p < 0.05$) and the control group (1.44 ± 0.28 *versus* 1.02 ± 0.24, $p < 0.05$) at Day 3. However, no significant difference existed between each of three experimental groups and control group at Day 7 [Figure 6(c)]. Here, a decrease in ROS expression in the HA-CeO_2-labeled HucMSC group at Day 7 could be partly due to the downregulation of iNOS and upregulation of Nrf2 in expressions.

HA-CeO_2-labeled HucMSCs carried the newly established effects of modulation on inflammation

These cytokines were selected to reflect the effects of modulation on inflammation from HA-CeO_2-labeled HucMSCs. At Day 7, the IFN-γ expression in the HA-CeO_2-labeled HucMSC group also decreased significantly when compared with the control group [0.07 ± 0.01 pg/mg *versus* 1.93 ± 0.43 pg/mg, $p = 0.008$; Figure 6(e)]. Moreover, At Day 7, differences of IL-6 expression existed between the HA-CeO_2-labeled HucMSC group and control group (0.94 ± 0.18 pg/mg *versus* 9.07 ± 2.99 pg/mg, $p = 0.032$), between the HA-CeO_2 group and the control group (2.61 ± 0.53 pg/mg *versus* 9.07 ± 2.99 pg/mg, $p = 0.045$). However, there was no obvious difference between the HucMSC group and control group [4.31 ± 1.66 pg/mg *versus* 9.07 ± 2.99 pg/mg, $p > 0.05$; Figure 6(g)]. The RANTES expression showed significant differences between some experimental groups and the control group. At both Day 2 and Day 7 after MCAO, RANTES expression was lower in the HA-CeO_2-labeled HucMSC group than the control group ($0.89 \pm 0.0.9$ pg/mg *versus* 1.55 ± 0.23 pg/mg $p = 0.032$ at Day 2; and 0.68 ± 0.19 pg/mg *versus* 3.18 ± 1.16 pg/mg, $p < 0.05$ at Day 7). RANTES expression was lower in the HA-CeO_2 group than the control group only at Day 7 [0.84 ± 0.15 pg/mg *versus* 3.18 ± 1.16 pg/mg, $p < 0.05$; Figure 6(h)].

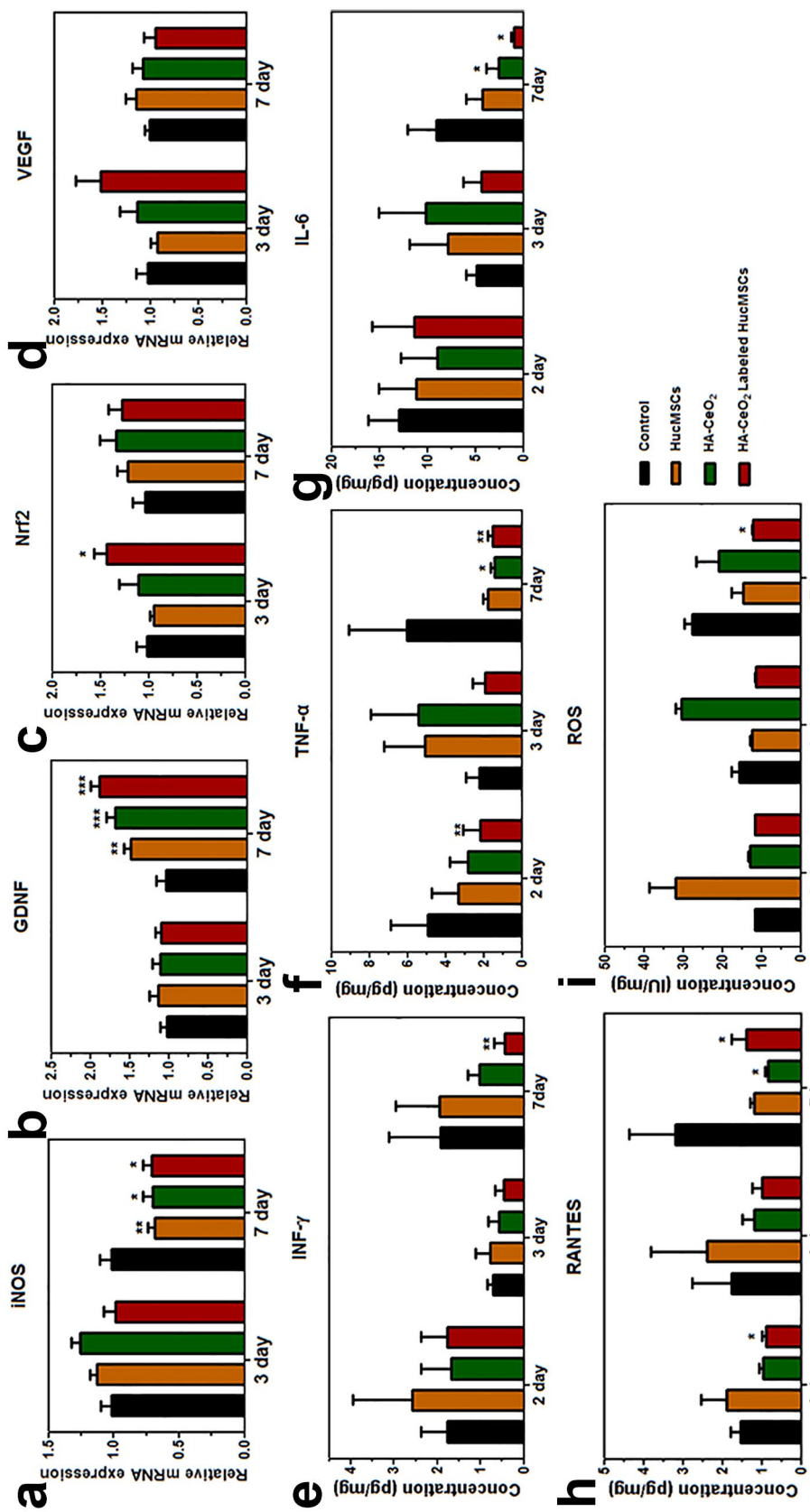

Figure 6. Antioxidative, inflammatory modulation and neurotrophic effects of HA-CeO_2-labeled HucMSCs. (a–d) Relative mRNA expression levels at Day 3 and Day 7 after MCAO in rat brain tissue of each group detected by real-time PCR. (a) iNOS; (b) GDNF; (c) Nrf2; (d) VEGF; (e–i) cytokine expression (pg/mg) and ROS expression (IU/mg) at Day 2, Day 3 and Day 7 after MCAO in rat brain tissues of each group detected by ELISA. (e) IFN-γ; (f) TNF-α; (g) IL-6; (h) RANTES; (i) ROS.

HA, hyaluronic acid; CeO2, nanoceria; HucMSCs, Human umbilical cord mesenchymal stem cells; mRNA, MCAO, middle cerebral artery occlusion; PCR, Polymerase Chain Reaction; iNOS, inducible nitric oxide synthase; GDNF,glial-derived neurotrophic factor; Nrf2, nuclear factor-erythroid-2-related factor 2; VEGF, vascular endothelial growth factor; ELISA, Enzyme-linked immunosorbent assay; IFN-γ, interferon-γ; TNF-α, umor necrosis factor -α; IL-6, Interleukin-6; RANTES, regulated upon activation normal T cell expressed and secreted; ROS, Reactive Oxygen Species.

$^{*}p < 0.05$
$^{**}p < 0.01$
$^{***}p < 0.005$.

TNF-α expression was lower in the HA-CeO_2-labeled HucMSC group than the control group at both Day 2 (2.17 ± 0.9 pg/mg *versus* 4.91 ± 1.6 pg/mg, $p = 0.009$) and Day 7 (0.58 ± 0.21 pg/mg *versus* 6.05 ± 1.83 pg/mg, $p = 0.004$) after MCAO. Similarly, TNF-α expression was also lower in the HA-CeO_2 group than the control group at Day 7 [1.43 ± 0.45 pg/mg *versus* 6.05 ± 1.83 pg/mg, $p = 0.016$; Figure 6(f)]. With the exception of the cytokines and chemokines described above, a significant difference for other cytokines was not found between each of experimental groups and control group at Day 2, 3 and 7 after MCAO. Remarkably, the immunomodulatory effect of HA-CeO_2-labeled HucMSCs was higher than that of HucMSCs and HA-CeO_2 at influencing the expression of inflammatory factors.

HA-CeO_2-labeled HucMSCs carried the enhanced effects of neurotrophy

Gene expressions of brain-derived neurotrophic factor (BDNF), neurotrophin 3 (NT-3), nerve growth factor (NGF) and glial-derived neurotrophic factor (GDNF) were measured with real-time PCR assay in the brain tissue of rats at Day 3 and 7 after MCAO. Expression level of GDNF significantly increased in all experimental groups when compared with that of the control group at Day 7 after MCAO (1.83 ± 0.27 *versus* 1.03 ± 0.30, $p = 0.001$ for the HA-CeO_2-labeled HucMSC group, 1.48 ± 0.20 *versus* 1.03 ± 0.30, $p = 0.021$ for the HucMSC group; and 1.68 ± 0.22 *versus* 1.03 ± 0.30, $p = 0.009$ for the HA-CeO_2 group). In addition, the expression level of GDNF was significant higher in the HA-CeO_2-labeled HucMSC group than the HucMSC group [$p = 0.029$; Figure 6(b)]. The expression level of GDNF had significant differences between the HA-CeO_2 group and control group at Day 7 (0.74 ± 0.22 *versus* 1.01 ± 0.16, $p = 0.03$). There was no significant difference for expression levels of other neurotrophic factors among all of four groups at Day 3 and Day 7 after MCAO.

HA-CeO_2-labeled HucMSCs had no detectable negative effect on the expression of VEGF

Real-time PCR assay was used to evaluate VEGF mRNA expression levels. Results showed that there was no significant difference between each of three experimental groups and control group at Day 3 and Day 7 after MCAO [$p > 0.05$, Figure 6(d)]. Our results prove that HA-CeO_2-labeled HucMSCs had no detectable negative effect for VEGF expressions, which suggested that the combination of HA-CeO_2 and HucMSCs probably has no negative effect on angiogenesis.

HA-CeO_2-labeled HucMSCs enhanced the anti-apoptosis effect

The effects of anti-apoptosis and neuroprotection for either MSCs or ceria were reported in several previous publications.[27,29,39] Here, we investigated whether HA-CeO_2-labeled HucMSCs combined the features of MSCs and ceria, and that HA-CeO_2-labeled HucMSCs could have an even enhanced anti-apoptosis effect. At Day 3 after MCAO, the percentages of apoptotic cells in each group were: $42.3\% \pm 10.5\%$ in the HA-CeO_2-labeled HucMSC group, $46.8\% \pm 10\%$ in the HucMSC group, $46.2\% \pm 7.1\%$ in the HA-CeO_2 group and $65.9\% \pm 10.4\%$ in the control group, respectively. The levels of apoptosis cells in each experimental group were less than that of the control groups ($p < 0.05$). Remarkably, the results of the TUNEL assay indicated the capacity of anti-apoptosis for HA-CeO_2-labeled HucMSCs was stronger than that for either HucMSCs or HA-CeO_2 under *in vivo* conditions, which were reflected by the finding of fewer apoptotic cells in brain tissues of rats after MCAO (Figure 7).

Discussion

In this study, we have successfully proved our hypothesis that MSCs combined with ceria will be more effective in the treatment of cerebral ischemia for inflammatory modulation and antioxidation.

For the combination between ceria and HucMSCs, nanoceria were precovered with HA at first. Afterward, HucMSCs were labeled with HA-CeO_2 on their cell surfaces through a HA subunit binding to the CD44 receptors. Next, the compatibilities of HucMSCs after HA-CeO_2 labeling were analyzed by MTT assay and surface markers, which proved the successful modification of HA-CeO_2 on HucMSCs. After success in these special steps of preparation, the effects of HA-CeO_2-labeled HucMSCs could be analyzed for ACI therapy *in vivo*. Remarkably, it was encouraging to find that HA-CeO_2-labeled HucMSCs significantly decreased the infarction volume and promoted the recoveries of both

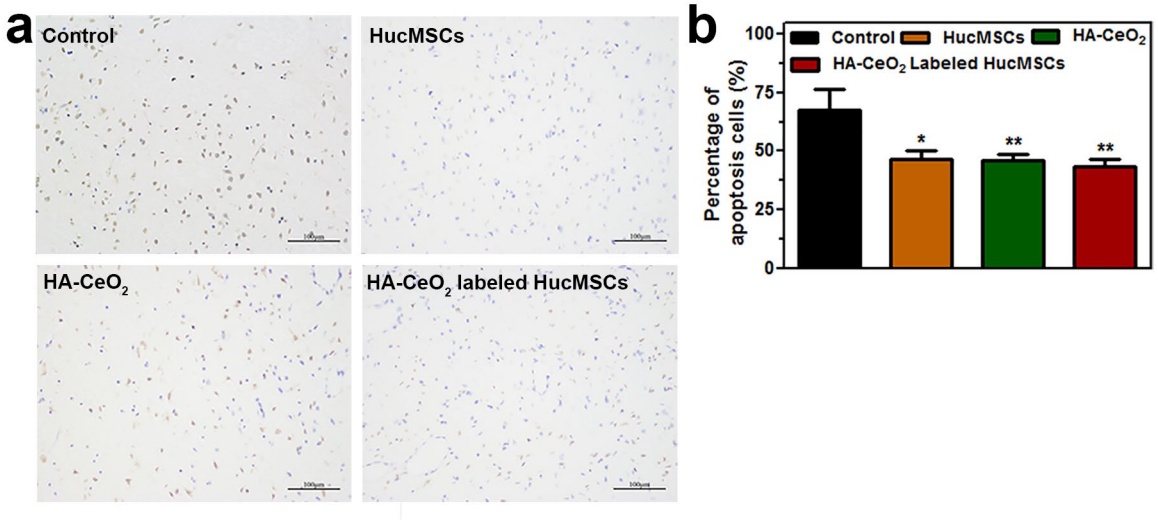

Figure 7. HA-CeO_2-labeled HucMSCs decreased apoptosis after cerebral ischemia reperfusion injury tested with a TUNEL assay. (a) Results of positive apoptosis staining of TUNEL assay on rat brain slice in each group (LM, ×200), Scale bar: 100 μM. (b) The percentage of apoptosis cells in each group.
HA, hyaluronic acid; CeO_2, nanoceria; HucMSCs, Human umbilical cord mesenchymal stem cells; TUNEL, TdT-mediated dUTP Nick-End Labeling.
*$p < 0.05$
**$p < 0.01$.

neurological and healthy parameters in the treated rat model of MCAO.

Results of our analyses to study the mechanism of the effects of HA-CeO_2-labeled HucMSCs for ACI therapy implied that antioxidant properties of HA-CeO_2-labeled HucMSCs was obtained through downregulation of iNOS and upregulation of Nrf2 at the levels of their gene expression. The expression of iNOS was upregulated under ischemic injury, which resulted in an increase of nitric oxide (NO) production. These findings could be explained by NO being a key factor acting during oxidative stress, which increases the formation of peroxynitrite.[40,41] Furthermore, activated Nrf2 could mediate the induced expression of an array of enzymes and signaling proteins to regulate antioxidant defense because Nrf2 has already been known previously as a key regulator of cellular resistance to oxidants.[42]

Our results also indicated that the immunomodulatory effect of HA-CeO_2-labeled HucMSC treatment was higher than that of either individual HucMSC treatment or individual HA-CeO_2 treatment, which included the effects of negatively influencing the expression of inflammatory factors including TNF-α, IFN-γ, IL-6 and RANTES. Remarkably, both TNF-α and IFN-γ are known as the important cytokines for inducing neuronal cell apoptosis.[43,44] Therefore, the decreased expression of both TNF-α and IFN-γ after the treatment of transplantation of HA-CeO_2-labeled HucMSCs could be beneficial to the rats after MCAO. IL-6 is known as another important cytokine involving in cerebral ischemia.[45] Previously, the elevated IL-6 level in serum was found in acute stroke patients, and was regarded to associate with infarct volume and prognosis.[45] But the results from some recent studies suggested that IL-6 might act as a neuroprotective cytokine in stroke.[46] The decreased expression of IL-6 found in the HA-CeO_2-labeled HucMSC-treated group during our study seemed to correlate more with the results in the improved neurological scores and the recovered animal body weights. However, these results were also not consistent with the previous realization of IL-6 acting as a neuronal protective agent. Therefore, the exact mechanism of decreased expression of IL-6 will be further investigated in our future study. RANTES is known as a chemokine that promotes the migration of leukocytes into damaged tissue and mediates cerebral inflammation and injury.[47] Here, our results of the downregulation of RANTES could be well explained by its consistence with the resultant decrease in injury after cerebral ischemia.

Our results of the neurotropic effects of HA-CeO_2-labeled HucMSCs were consistent with previously published findings.[48] Nicole and colleagues indicated that the neuroprotection of GDNF involved in the reduction of N-methyl-D-aspartic acid (NMDA)-induced calcium influx. In addition, it was also possible that the persistently elevated GDNF and VEGF could increase neurogenesis and angiogenesis.[49] The details of how HA-CeO_2-labeled HucMSCs performed the enhanced effects of neuroprotection are expected to be elucidated in our subsequent study.

Gliga and colleagues[50] reported that nanoceria could inhibit neuronal differentiation *in vitro* because nanoceria interfered with the expression of β3-tubulin and Glial fibrillary acidic protein (GFAP), and this inhibition effect partly related to the antioxidant properties of nanoceria. In addition, because endogenous neurogenesis is one of the important mechanisms after stem cell transplantation to the rat ischemic stroke model, the downregulation of genes relative to neurogenesis may influence the long-term recovery of stroke animals. The different effects of nanoceria may also relate to the different doses, the different sizes, and the differences in shape of particles and ratios of Ce^3+ to Ce^4+. Therefore, the effects of HA-CeO_2 or HA-CeO_2-labeled HucMSCs on neurogenesis will be further investigated in our future study.

Conclusion

In conclusion, we generated nanoceria that have considerable biocompatibility and promising scavenging activity of intracellular ROS. The nanoceria-labeled HucMSCs have the combined advantages from two original units (individual HucMSC and nanoceria) after the modification of cell labeling, which are the capacity of inflammation responses for HucMSCs and antioxidant effects for nanoceria. Moreover, we have proven that nanoceria-labeled HucMSCs have significantly enhanced antioxidant, inflammatory modulation, anti-apoptosis and neurotrophy properties when compared with applying HucMSCs and nanoceria before the cell labeling modification. Therefore, our study provides a new insight into the interface between nanotechnology and medicine for clinical applications. Our findings also suggest that transplantation of nanoceria-labeled HucMSCs could be used as a novel strategy for the effective and well-tolerated treatment of ACI in the future.

Acknowledgments

We are very grateful to Professor Yufang Shi and his team for providing HucMSCs.

Lian Zuo and Qishuai Feng contributed equally to this article.

All applicable international, national and institutional guidelines for the care and use of animals were followed.

Funding

The authors disclosed receipt of the following financial support for the research, authorship, and/or publication of this article: This work was supported by grants obtained from the Ministry of Science and Technology (No. 2016YFA0101301), Shanghai Science and Technology Commission (No.16511105000-16511105002), Key Disciplines Group Construction Project of Pudong Health Bureau of Shanghai (No.PWZxp2017-08), Clinical Peak Discipline Construction Project of Pudong New Area Government (No. PWYgf2018-05) and National Science Foundation of China (Grant No. 81601010).This work was also supported by National Science Foundation of China (No.81571803). Y.C. thanks the Thousand Talents Plan, Shanghai Municipal Education Commission Innovative Program (No.2017-01-07-00-07-E00038), and Shanghai Science and International Cooperation Program (No.16410724300).

Conflict of interest statement

The authors declare that there is no conflict of interest.

ORCID iD

Gang Li https://orcid.org/0000-0003-1737-0107

References

1. Powers WJ, Derdeyn CP, Biller J, *et al.* American Heart Association/American Stroke Association focused update of the 2013 guidelines for the early management of patients with acute ischemic stroke regarding endovascular treatment: a guideline for healthecare professionals from the American Heart Association/American Stroke Association. *Stroke* 2015; 46: 3020–3035.

2. Nogueira RG, Jadhav AP, Haussen DC, *et al.* Thrombectomy 6 to 24 hours after stroke with a mismatch between deficit and infarct. *N Engl J Med* 2018; 378: 11–21.
3. Albers GW, Marks MP, Kemp S, *et al.* Thrombectomy for stroke at 6 to 16 hours with selection by perfusion imaging. *N Engl J Med* 2018; 378: 708–718.
4. The STEPS Participants. Stem cell therapies as an emerging paradigm in stroke (STEPS): bridging basic and clinical science for cellular and neurogenic factor therapy in treating stroke. *Stroke* 2009; 40: 510–515.
5. Romanko MJ, Rola R, Fike JR, *et al.* Roles of the mammalian subventricular zone in cell replacement after brain injury. *Prog Neurobiol* 2004; 74: 77–99.
6. Arvidsson A, Collin T, Kirik D, *et al.* Neuronal replacement from endogenous precursors in the adult brain after stroke. *Nat Med* 2002; 8: 963–970.
7. Gervois P, Wolfs E, Ratajczak J, *et al.* Stem cell-based therapies for ischemic stroke: preclinical results and the potential of imaging-assisted evaluation of donor cell fate and mechanisms of brain regeneration. *Med Res Rev* 2016; 36: 1080–1126.
8. Su J, Chen X, Huang Y, *et al.* Phylogenetic distinction of iNOS and IDO function in mesenchymal stem cell-mediated immunosuppression in mammalian species. *Cell Death Differ* 2014; 21: 388–396.
9. Honmou O, Onodera R, Sasaki M, *et al.* Mesenchymal stem cells: therapeutic outlook for stroke. *Trends Mol Med* 2012; 18: 292–297.
10. Newman MB, Willing AE, Manresa JJ, *et al.* Cytokines produced by cultured human umbilical cord blood(HUCB) cells: implications for brain repair. *Exp Neurol* 2006; 199: 201–208.
11. Vu Q, Xie K, Eckert M, *et al.* Meta-analysis of preclinical studies of mesenchymal stromal cells for ischemic stroke. *Neurology* 2014; 82: 1277–1286.
12. Li Y, Chen J, Zhang CL, *et al.* Gliosis and brain remodeling after treatment of stroke in rats with marrow stromal cells. *Glia* 2005; 49: 407–417.
13. Bang OY, Lee JS, Lee PH, *et al.* Autologous mesenchymal stem cell transplantation in stroke patients. *Ann Neurol* 2005; 57: 874–882.
14. Bhasin A, Srivastava MV, Mohanty S, *et al.* Stem cell therapy: a clinical trial of stroke. *Clin Neurol Neurosurg* 2013; 115: 1003–1008.
15. Honmou O, Houkin K, Matsunaga T, *et al.* Intravenous administration of auto serum-expanded autologous mesenchymal stem cells in stroke. *Brain* 2011; 134: 1790–1807.
16. Savitz SI, Misra V, Kasam M, *et al.* Intravenous autologous bone marrow mononuclear cells for ischemic stroke. *Ann Neurol* 2011; 70: 59–69.
17. Nagpal A, Choy FC, Howell S, *et al.* Safety and effectiveness of stem cell therapies in early-phase clinical trials in stroke: a systematic review and meta-analysis. *Stem Cell Res Ther* 2017; 8: 191.
18. Wang Q, Duan F, Wang MX, *et al.* Effect of stem cell-based therapy for ischemic stroke treatment: a meta-analysis. *Clin Neurol Neurosurg* 2016; 146: 1–11.
19. Wei L, Wei ZZ, Jiang MQ, *et al.* Stem cell transplantation therapy for multifaceted therapeutic benefits after stroke. *Prog Neurobiol* 2017; 157: 49–78.
20. Kurozumi K, Nakamura K, Tamiya T, *et al.* BDNF gene-modified mesenchymal stem cells promote functional recovery and reduce infarct size in the rat middle cerebral artery occlusion model. *Mol Ther* 2004; 9: 189–197.
21. Horita Y, Honmou O, Harada K, *et al.* Intravenous administration of glial cell line-derived neurotrophic factor gene-modified human mesenchymal stem cells protects against injury in cerebral ischemia model in the adult rat. *J Neurosci Res* 2006; 84: 1495–1504.
22. Liu H, Honmou O, Harada K, *et al.* Neuroprotection by PlGF gene-modified human mesenchymal stem cells after cerebral ischaemia. *Brain* 2006; 129: 2734–2745.
23. Tsai LK, Wang Z, Munasinghe J, *et al.* Mesenchymal stem cells primed with valproate and lithium robustly migrate to infarcted regions and facilitate recovery in a stroke model. *Stroke* 2011; 42: 2932–2939.
24. Kaengkan P1, Baek SE, Kim JY, *et al.* Administration of mesenchymal stem cells and ziprasidone enhanced amelioration of ischemic brain damage in rats. *Mol Cells* 2013; 36: 534–541.
25. Chung TN, Kim JH, Choi BY, *et al.* Effect of adipose-derived mesenchymal stem cell administration and mild hypothermia induction on delayed neuronal death after transient global cerebral ischemia. *Crit Care Med* 2017; 45: e508–e515.
26. Karakoti A, Singh S, Dowding JM, *et al.* Redox-active radical scavenging nanomaterials. *Chem Soc Rev* 2010; 39: 4422.

27. Lee SS, Song W, Cho M, *et al*. Antioxidant properties of cerium oxide nanocrystals as a function of nanocrystal diameter and surface coating. *ACS Nano* 2013; 7: 9693–9703.

28. Selvaraj V, Nepal N, Rogers S, *et al*. Inhibition of MAP kinase/NF-kB mediated signaling and attenuation of lipopolysaccharide induced severe sepsis by cerium oxide nanoparticles. *Biomaterials* 2015; 59: 160.

29. Mitra RN, Gao R, Zheng M, *et al*. Glycol chitosan engineered autoregenerative antioxidant significantly attenuates pathological damages in models of age-related macular degeneration. *ACS Nano* 2017; 11: 4669–4685.

30. Kim CK, Kim T, Choi IY, *et al*. Ceria nanoparticles that can protect against ischemic stroke. *Angew Chem Int Ed Engl* 2012; 124: 11201–11205.

31. Popov AL, Zaichkina SI, Popova NR, *et al*. Radioprotective effects of ultra-small citrate-stabilized cerium oxide nanoparticles in vitro and in vivo. *RSC Adv* 2016, 6: 106141–106149.

32. Lee SS, Zhu H, Contreras EQ, *et al*. High temperature decomposition of cerium presursors to form ceria nanaocrystal libraries for biological applications. *Chem Mater* 2012; 3: 424–432.

33. Longa EZ, Weinstein PR, Carlson S, *et al*. Reversible middle cerebral artery occlusion without craniectomy in rats. *Stroke* 1989; 20: 84–91.

34. Chang CF, Lin SZ, Chiang YH, *et al*. Intravenous administration of bone morphogenetic protein-7 after ischemia improves motor function in stroke rats. *Stroke* 2003; 34: 558–564.

35. Desland FA, Afzal A, Warraich Z, *et al*. Manual versus automated rodent behavioral assessment: comparing efficacy and ease of Bederson and Garcia neurological deficit scores to an open field video-tracking system. *J Cent Nerv Syst Dis* 2014; 6: 7–14.

36. Swanson RA, Morton MT, Tsao-Wu G, *et al*. A semiautomated method for measuring brain infarct volume. *J Cereb Blood Flow Metab* 1990; 10: 290–293.

37. Knauss S, Endres M, Blaschke F, *et al*. Oral administration of a novel lipophilic PPARδ agonist is not neuroprotective after rodent cerebral ischemia. *J Cereb Blood Flow Metab* 2018; 38: 174–185.

38. Tang X, Liu K, Hamblin MH, *et al*. Genetic deletion of Krüppel-like factor 11 aggravates ischemic brain injury. *Mol Neurobiol* 2018; 55: 2911–2921.

39. Chelluboina B, Klopfenstein JD, Pinson DM, *et al*. Stem cell treatment after cerebral ischemia regulates the gene expression of apoptotic molecules. *Neurochem Res* 2014; 39: 1511–1521.

40. Han HS, Qiao Y, Karabiyikoglu M, *et al*. Influence of mild hypothermia on inducible nitric oxide synthase expression and reactive nitrogen production in experimental stroke and inflammation. *J Neurosci* 2002; 22: 3921–3928.

41. Liu PK, Grossman RG, Hsu CY, *et al*. Ischemic injury and faulty gene transcripts in the brain. *Trends Neurosci* 2001; 24: 581–588.

42. Ma Q. Role of nrf2 in oxidative stress and toxicity. *Annu Rev Pharmacol Toxicol* 2013; 53: 401–426.

43. Liesz A, Suri-Payer E, Veltkamp C, *et al*. Regulatory T cells are key cerebroprotective immunomodulators in acute experimental stroke. *Nat Med* 2009; 15: 192–199.

44. Shichita T, Sakaguchi R, Suzuki M, *et al*. Post-ischemic inflammation in the brain. *Front Immunol* 2012; 3: 132.

45. Smith CJ, Emsley HC, Gavin CM, *et al*. Peak plasma interleukin-6 and other peripheral markers of inflammation in the first week of ischaemic stroke correlate with brain infarct volume, stroke severity and long-term outcome. *BMC Neurol* 2004; 4: 2.

46. Suzuki S, Tanaka K and Suzuki N. Ambivalent aspects of interleukin-6 in cerebral ischemia: inflammatory versus neurotrophic aspects. *J Cereb Blood Flow Metab* 2009; 29: 464–479.

47. Terao S, Yilmaz G, Stokes KY, *et al*. Blood cell-derived RANTES mediates cerebral microvascular dysfunction, inflammation, and tissue injury after focal ischemia-reperfusion. *Stroke* 2008; 39: 2560–2570.

48. Nicole O, Ali C, Docagne F, *et al*. Neuroprotection mediated by glial cell line-derived neurotrophic factor: involvement of a reduction of NMDA-induced calcium influx by the mitogen-activated protein kinase pathway. *J Neurosci* 2001; 21: 3024–3033.

49. Doeppner TR, Traut V, Heidenreich A, *et al*. Conditioned medium derived from neural progenitor cells induces long-term post-ischemic neuroprotection, sustained neurological recovery, neurogenesis, and angiogenesis. *Mol Neurobiol* 2017; 54: 1531–1540.

50. Gliga AR, Edoff K, Caputo F, *et al*. Cerium oxide nanoparticles inhibit differentiation of neural stem cells. *Sci Rep* 2017; 7: 9284.